Supporting Information

Interplay of Fluorescence and Phosphorescence in Organic Biluminescent Emitters

Caterin Salas Redondo, [1,2] *Paul Kleine,* [1] *Karla Roszeitis,* [1] *Tim Achenbach,* [1] *Martin Kroll,* [1] *Michael Thomschke,* [1] *and Sebastian Reineke** [1,2]

[1] Dresden Integrated Center for Applied Physics and Photonic Materials (IAPP) and Institute for Applied Physics, Technische Universität Dresden, Nöthnitzer Straße 61, D-01187, Germany

[2] Center for Advancing Electronics Dresden (cfaed), Technische Universität Dresden, Würzburger Straße 46, D-01187 Dresden, Germany

AUTHOR INFORMATION

Corresponding Author

*Sebastian Reineke. E-mail: reineke@iapp.de

CONTENT

1. Detailed calculation of the photoluminescence transients

For each system composition (i.e. $[PMMA:NPB]_{sc}$, $[TCTA:NPB]_{sc}$ and $[TCTA:NPB]_{evap}$), two identical samples are made, which are fitted independently using:

$$I = A_1 e^{-(t/\tau_1)} + A_2 e^{-(t/\tau_2)} + A_{\mathrm{bg}} \quad (1)$$

Where A_1 and A_2 are the relative contributions of the individual decays with lifetimes τ_1 and τ_2, respectively. A_{bg} is a constant offset that describes the instrument background intensity.

Afterwards, the average weighted lifetimes $\acute{\tau}$ are calculated according to:

$$\hat{\tau} = \frac{A_1}{A_1+A_2}\tau_1 + \frac{A_2}{A_1+A_2}\tau_2. \quad (2)$$

Finally, the mean value of the lifetimes $\hat{\tau}_{\mathrm{av}}$ are calculated out of the results of the two samples per system. The final results are given here as well as in the main text (cf. Table 1). Moreover, we present in Tables S1 and S2 the values of all the parameters obtained after the fitting process to find both, the fluorescence (Table S1a-c) and phosphorescence (Table S2a-c) lifetimes.

Data corresponding to the fitting of fluorescence lifetime:

Table S1a. Summary of the fluorescence lifetime fitting of $[PMMA:NPB]_{sc}$

Sample	Atmosphere	A_{bg}	A_1	τ_1 (ns)	A_2	τ_2 (ns)	$\hat{\tau}$ (ns)	$\hat{\tau}_{av}$ (ns)
A	Nitrogen	0	0.67	1.8	0.34	4.3	2.6	2.6
B		0	0.67	1.8	0.34	4.3	2.6	
A	Air	0	0.70	1.6	0.31	4.1	2.4	2.6
B		0	0.59	1.7	0.43	4.2	2.7	

Table S1b. Summary of the fluorescence lifetime fitting of $[TCTA:NPB]_{sc}$

Sample	Atmosphere	A_{bg}	A_1	τ_1 (ns)	A_2	τ_2 (ns)	$\hat{\tau}$ (ns)	$\hat{\tau}_{av}$ (ns)
C	Nitrogen	0	0.62	4.0	0.39	1.7	3.1	3.4
D		0	0.92	3.1	0.12	7.4	3.6	
C	Air	0	0.72	2.5	0.28	4.9	3.2	3.4
D		0	0.76	2.8	0.24	5.9	3.5	

Table S1c. Summary of the fluorescence lifetime fitting of $[TCTA:NPB]_{evap}$

Sample	Atmosphere	A_{bg}	A_1	τ_1 (ns)	A_2	τ_2 (ns)	$\hat{\tau}$ (ns)	$\hat{\tau}_{av}$ (ns)
E	Nitrogen	0	0.25	3.8	0.76	1.4	2.0	2.0
F		0	0.78	1.5	0.23	3.6	2.0	
E	Air	0	0.27	3.7	0.74	1.4	2.0	2.3
F		0	0.24	4.2	0.77	2.0	2.5	

On the same regard, the complete data obtained from the fitting of the phosphorescence is then:

Table S2a. Summary of the phosphorescence lifetime fitting of $[PMMA:NPB]_{sc}$

Sample	Atmosphere	A_{bg}	A_1	τ_1 (ms)	A_2	τ_2 (ms)	$\hat{\tau}$ (ms)	$\hat{\tau}_{av}$ (ms)
A	Nitrogen	0	0.10	17.5	0.9	382.2	346.3	322.6
B		0	0.12	22.0	0.88	337.2	298.8	
A	Air	0.06	0.83	7.4	0.11	34.6	10.7	10.4
B		0.06	0.75	5.3	0.19	28.9	10.0	

Table S2b. Summary of the phosphorescence lifetime fitting of $[TCTA:NPB]_{sc}$

Sample	Atmosphere	A_{bg}	A_1	τ_1 (ms)	A_2	τ_2 (ms)	$\hat{\tau}$ (ms)	$\hat{\tau}_{av}$ (ms)
C	Nitrogen	0	0.36	12.5	0.64	162.4	108.6	95.6
D		0	0.38	11.3	0.62	125.9	82.5	
C	Air	0.06	0.84	6.0	0.10	46.1	10.2	10.1
D		0.06	0.85	6.3	0.09	45.6	10.0	

Table S2c. Summary of the phosphorescence lifetime fitting of $[TCTA:NPB]_{evap}$

Sample	Atmosphere	A_{bg}	A_1	τ_1 (ms)	A_2	τ_2 (ms)	$\hat{\tau}$ (ms)	$\hat{\tau}_{av}$(ms)
E	Nitrogen	0	0.44	11.0	0.56	102.8	62.0	53.8
F		0	0.53	9.9	0.47	86.0	45.5	
E	Air	0.2	0.47	13.3	0.53	2.2	7.5	7.1
F		0.05	0.13	25.1	0.87	4.0	6.7	

Furthermore, a set of decay curves that represent the fluorescence and phosphorescence transients under air and nitrogen atmospheres, with their equivalent curve fittings to align theoretical curves with normalized experimental transients are given below:

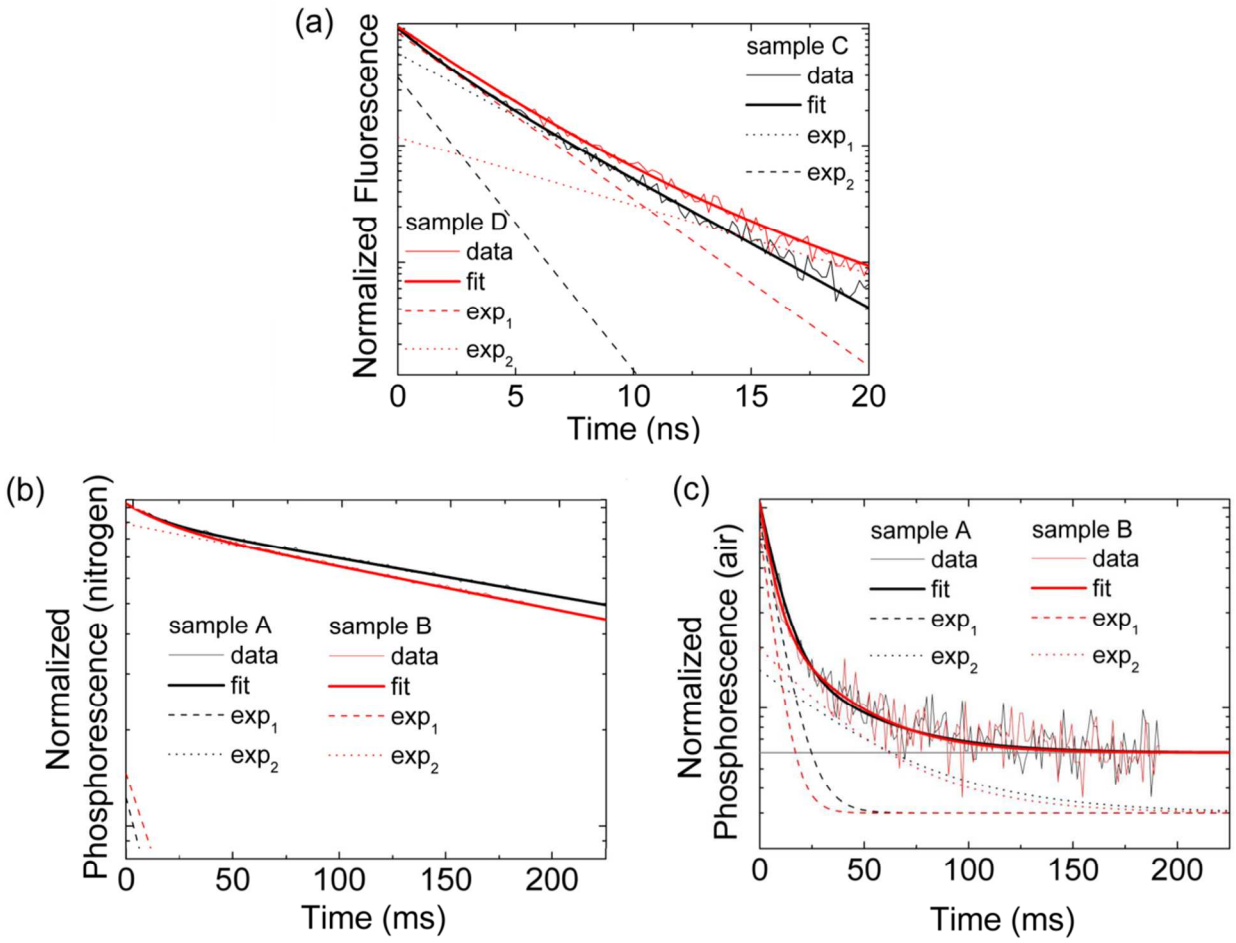

Figure S1. Typical double exponential fitting curves of the transient response. Solid bold line represents the double exponential fit, dashed and dotted lines correspond to the two monoexponential components exp_1 and exp_2 respectively. (a) Fit of the fluorescence transient of $[TCTA:NPB]_{sc}$ samples C (black) and D (red). (b) Fit of the phosphorescence transient in nitrogen of $[PMMA:NPB]_{sc}$ samples A (black) and B (red). (c) Fit of the phosphorescence transient in air of $[PMMA:NPB]_{sc}$ samples A (black) and B (red), the grey line represents the background level of the measurement system.

2. Morphology analysis of the biluminescent system TCTA:NPB

We have investigated the morphology of the biluminescence systems $[TCTA:NPB]_{sc}$ and $[TCTA:NPB]_{evap}$ with X-ray diffraction and Fourier transform infrared spectroscopy, in order to determine whether there are significant differences affecting the exciton dynamics of the biluminescent emitter NPB, depending on the technique we used to deposit the films.

Figures S2a and S2b are dedicated to the X-ray-reflectometry (XRR) and Grazing Incidence X-ray diffraction (GIXRD) of the films, respectively. The density of thin films can be estimated from the critical angle θ_c for total reflection of the signal in the XRR method [1] (cf. Figure S2a). Here, a shift in the total reflection edge is not apparent between both XRR signals, which implies that if at all, there is no significant change in density. Although the film density yielded to similar estimation, this does not suggest a similar local rigidity around the NPB molecules.

The GIXRD spectrum was obtained with incidence angles of 0.2095° and 0.184° for the TCTA:NPB spin coated and evaporated samples respectively. The diffraction peaks are not sharp for both vacuum-deposited and spin-coated films (cf. Figure S2b), indicating that no crystallization is present in the films [2] but rather they describe the profile of a disorder lattice of amorphous materials. This leads us to the conclusion that no aggregation or crystallization was induced in none of the samples.

According to the Fourier transform infrared spectroscopy (FTIR) spectra of TCTA:NPB films, deposited via spin coating (red) and evaporation (blue) techniques, the vibration modes are not influenced by the processing technique, but it rather presents different magnitudes throughout the IR spectrum (cf. Figure S2c), which indicates different concentration of bonds that contribute to each frequency [3.] We have selected the fingerprint region (from about 1500 to 500 cm^{-1}) for comparison, because this is the region of the IR in which a distinct pattern to each different

compound is produced [3] and therefore, by observing similar spectrum for both samples (spin coated and thermal evaporated) we are able to prove that the molecules are not affected by the processing technique.

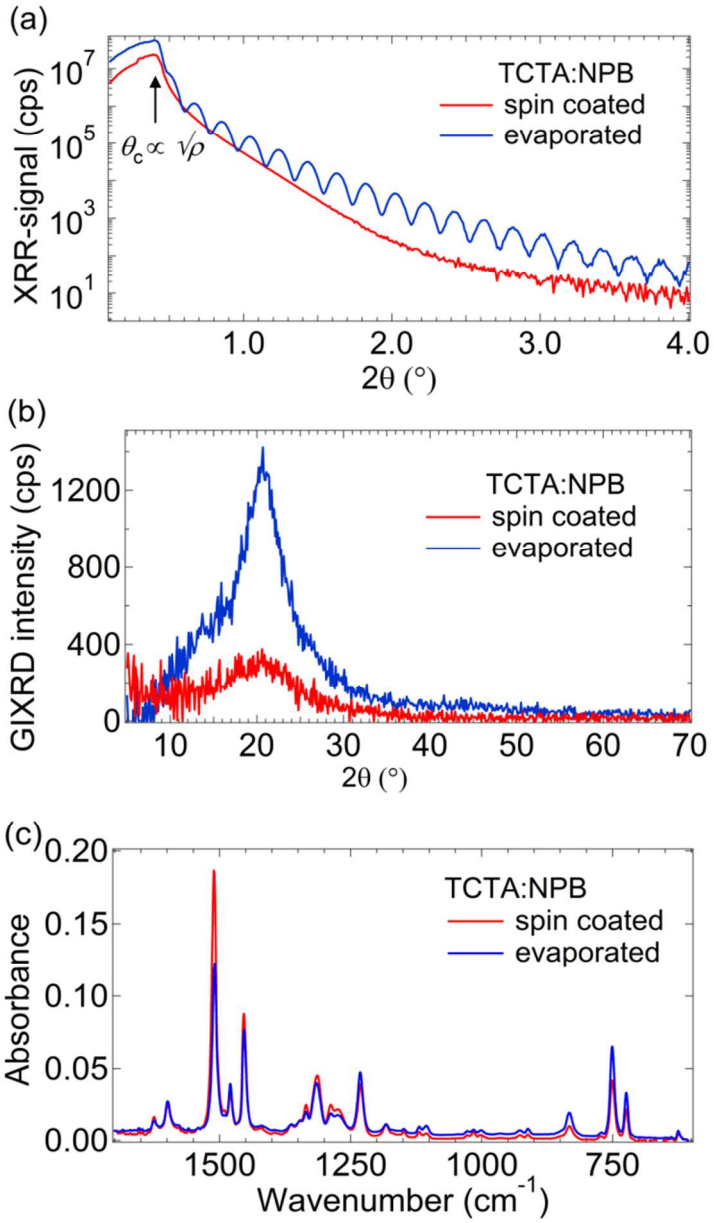

Figure S2. Morphology comparison of $[TCTA:NPB]_{sc}$ (red) and $[TCTA:NPB]_{evap}$ (blue) films. (a) X-Ray Reflectivity (XRR) indicating the critical angle θ_c at the total reflection edge of the XRR signal. (b) Grazing Incidence X-ray Diffraction (GIXRD) demonstrating broad diffraction peaks for both systems at $2\theta \sim 22°$. (c) Fourier transform infrared spectroscopy (FTIR) showing the absorbance in the fingerprint region (1500 to 500 cm^{-1}), obtained in Attenuated total reflection (ATR) mode.

3. TTA-based delayed fluorescence

We have observed delayed fluorescence in the delayed PL spectra (cf. Figure S3), which we appoint to annihilation-based up-conversion (triplet-triplet-annihilation) [4,5]. According to the PL spectra, the delayed fluorescence is as high as 50, 33, and 0.5% the phosphorescence of $[TCTA:NPB]_{evap}$ (blue), $[TCTA:NPB]_{sc}$ (red), and PMMA:NPB (black), respectively. We fitted the experimental data of the fluorescence spectra for all systems to the delayed fluorescence (DF) peak. From the observations, we can deduce that in all cases, the delayed fluorescence does not show a spectral shift compared to the fluorescence emission. However, the fluorescence spectrum in TCTA:NPB system showed a slight red shifted emission compared to that of PMMA:NPB system, indicating a presence of interactions between NPB molecule and TCTA matrix. For example, in the case of PMMA:NPB system, the singlet excitons are directly generated by light-absorption, but in the TCTA:NPB system, singlet excitons of NPB are mostly created through a resonance energy transfer from singlet of TCTA to singlet of NPB because excitation light is mainly absorbed by TCTA host molecules, as shown Figure S4a and S4b. Moreover, the overlap between the emission of TCTA and absorbance of NPB is favorable for a donor (TCTA)-acceptor (NPB) energy transfer case (cf. Figure S4c).

The interaction between nearby excited TCTA and NPB molecules yield to such annihilation process, which contributes to the effective non radiative decay $k_{nr,P}$, limiting the phosphorescence lifetime (cf. Figure 2b) producing a multi-exponential triplet state decay, also, representing the bimolecular process.

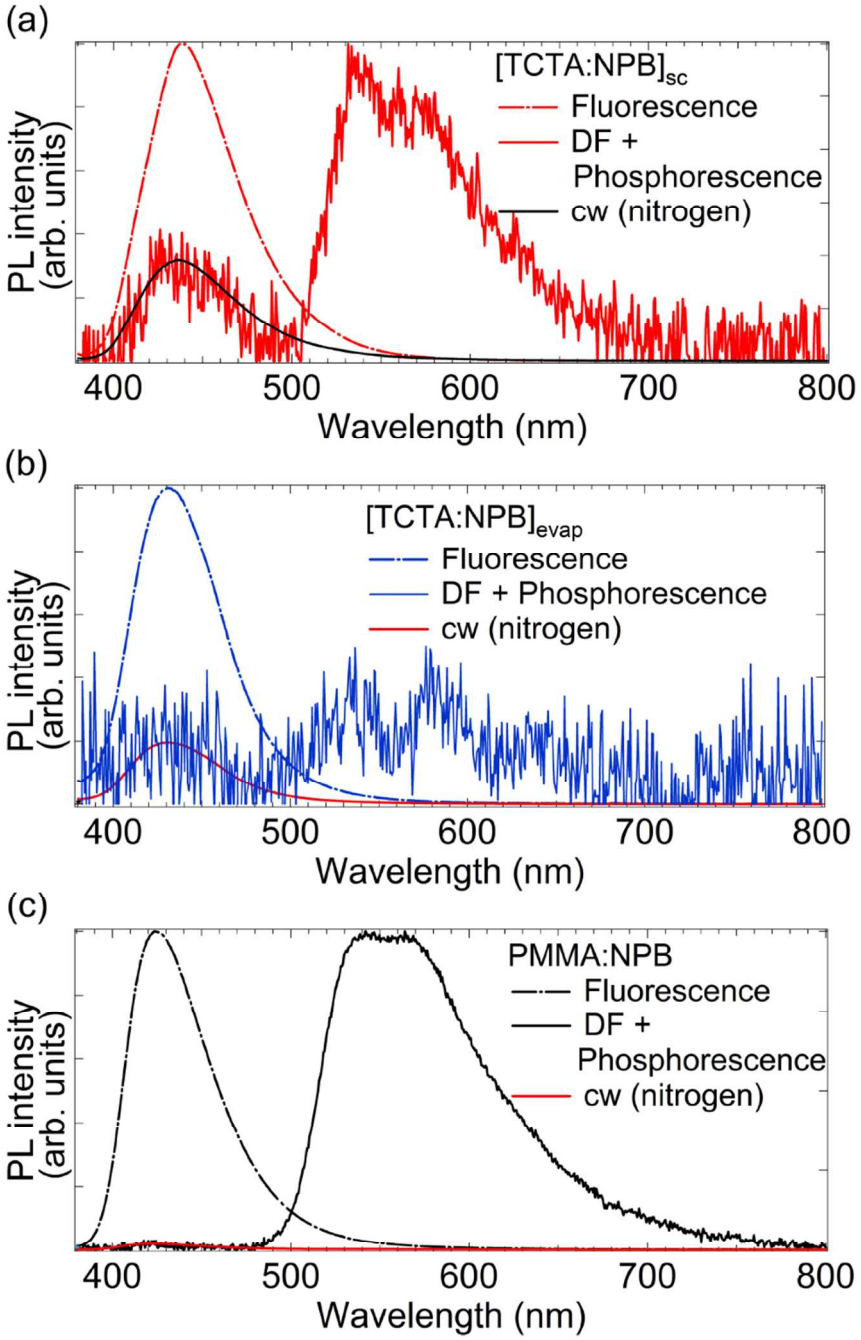

Figure S3. Continuous wave (fluorescence, dashed line) and gated (delayed fluorescence "DF" and phosphorescence) photoluminescence spectra under nitrogen atmosphere at room temperature of (a) $[TCTA:NPB]_{sc}$ (red), (b) $[TCTA:NPB]_{evap}$ (blue) and (c) $[PMMA:NPB]_{sc}$ (black). The delayed spectrum of all systems includes their fluorescence spectrum (cw (nitrogen)) with the aim of fitting it to its counterpart delayed fluorescence.

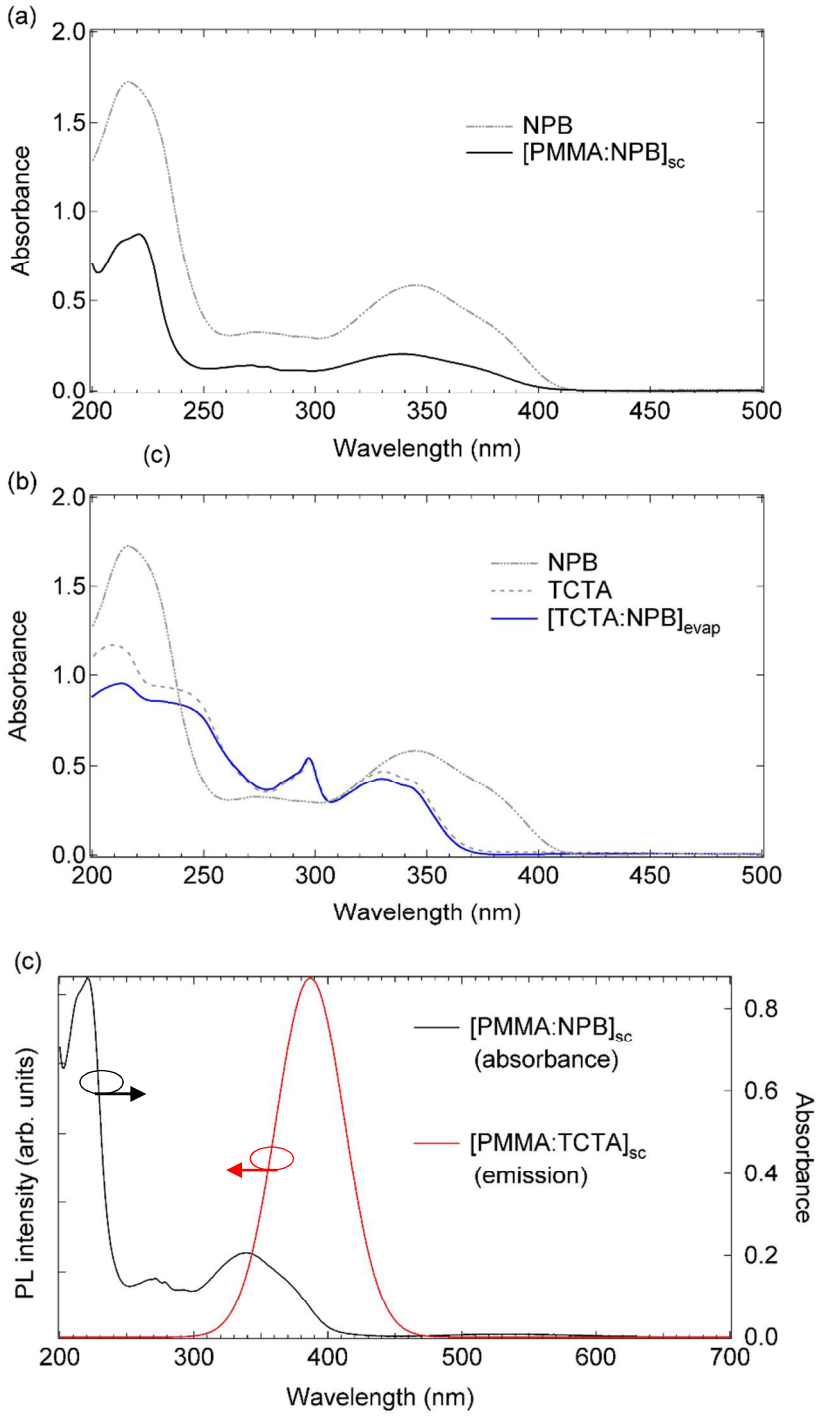

Figure S4. Absorbance spectrum of (a) NPB (grey dotted line), $[PMMA:NPB]_{sc}$ (black line), (b) TCTA (grey dashed line), and $[TCTA:NPB]_{evap}$ (blue line) thin films. $[TCTA:NPB]_{sc}$ reveals identical absorbance spectrum as its evaporated counterpart, therefore, it is not displayed here for clarity. (c) Overlap between absorbance spectrum of NPB (black line) and emission spectrum of TCTA (red line).

4. Calculation of the fluorescence and phosphorescence quantum yield

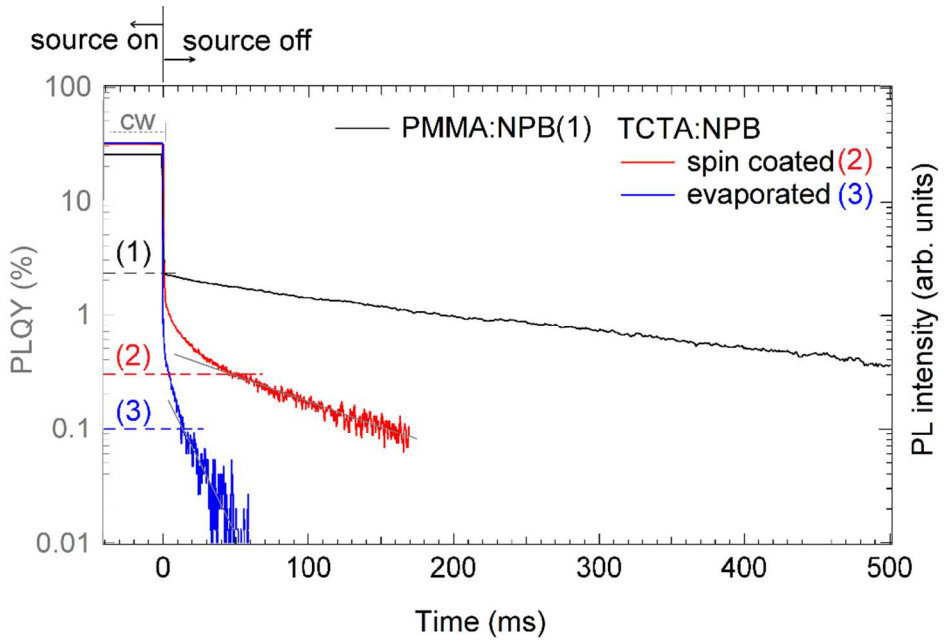

Figure S5. Time dependent emission profile of biluminescent films of NPB embedded in PMMA (black), spin coated TCTA (red) and thermal evaporated TCTA (blue). Phosphorescence transients following a pulsed LED with periods of 1 s, 300 ms and 100 ms for $[PMMA:NPB]_{sc}$, $[TCTA:NPB]_{sc}$ and $[TCTA:NPB]_{evap}$ samples, respectively, and 50% duty cycle. Data of the respective samples under cw-illumination (data points when time < 0) are scaled to the PL quantum yield (PLQY, grey y-axis). Labels (1), (2) and (3) correspond to the phosphorescence quantum yield ($PLQY_P$) of $[PMMA:NPB]_{sc}$, $[TCTA:NPB]_{sc}$ and $[TCTA:NPB]_{evap}$, respectively.

The intensity at -460 ms < time < 0 (source on), corresponds to the total emission of singlet (fluorescence) and triplet (phosphorescence) at steady state under cw-illumination. Since the PLQY is also obtained by integrating the total intensity of fluorescence and phosphorescence under cw-illumination during 1 s, which is enough for the systems to reach steady state, one can assume that the PL intensity at -460 ms < time < 0 (source on) is related to the PLQY. Therefore, the PL intensity of each system is normalized to their corresponding PLQY in order to estimate the fluorescence ($PLQY_F$) and phosphorescence ($PLQY_P$) yields as follows.

When time > 0 (source off), the long lived phosphorescence is observed. The value at the phosphorescence onset corresponds to the initial phosphorescence intensity which at the same time is related to $PLQY_P$. The phosphorescence decay of $[TCTA:NPB]_{sc}$ and $[TCTA:NPB]_{evap}$ is multi-exponential, due to the TTA-based delayed fluorescence (cf. Figure S3), which influences the shape during the first milliseconds, therefore, the chosen $PLQY_P$ value is extracted out of the contribution from the linear part of the decay. Finally, the fluorescence yield is the remaining part of the PLQY as follows:

$$PLQY_F = PLQY - PLQY_P \quad (3)$$

All values are summarized in Table S3:

Table S3. Summary of the contributions of fluorescence and phosphorescence to the PLQY of biluminescent systems.

System	PLQY [%]	$PLQY_F$	$PLQY_P$
$[PMMA:NPB]_{sc}$	26±3	23.7	2.3
$[TCTA:NPB]_{sc}$	31±8	30.7	0.3
$[TCTA:NPB]_{evap}$	32±3	31.9	0.1

Although, we can obtain a rough estimation of the fluorescence and phosphorescence yield using this technique, it is not completely accurate, because here, we assume that the samples have the same absorption in both measurements (PLQY and time resolved PL), which is not true, although the integration time was the same, the excitation power are not equal in both cases and the phosphorescence onset is arbitrarily chosen. Therefore, to obtain a more precise value, the phosphorescence yield can be calculated as follows. The PLQY represents the total efficiency of

the system, in order to calculate the separate phosphorescence and fluorescence efficiencies, one must separate both emissions spectra completely. If the total emission of fluorescence and phosphorescence is defined as the total integrated spectrum at every wavelength ($380 < \lambda < 800$ nm) in steady state during cw-illumination (I_{TOTAL}), and at the same time, the total emission intensity at every wavelength ($380 < \lambda < 800$ nm) after the excitation source is off is defined as the delayed intensity ($I_{DELAYED}$), which corresponds to the phosphorescence (I_P) and delayed fluorescence (I_{DF}) emissions. Then, the delayed yield can be calculated as:

$$\mathrm{PLQY_D} = \mathrm{PLQY}\left(\frac{I_{\mathrm{DELAYED}}}{I_{\mathrm{TOTAL}}}\right) \quad (4)$$

Additionally, we can assign the contributions of both delayed fluorescence (A_{DF}) and phosphorescence (A_P) to the fractions of short and long lifetime components (i.e. A_1 and A_2 of Equation (1)) for each corresponding phosphorescence transient data, respectively. Finally, the phosphorescence yield is computed using Equation (5):

$$\mathrm{PLQY_P} = A_P\mathrm{PLQY_D} \quad (5)$$

In this method, one must ensure that the spectra I_{TOTAL} and $I_{DELAYED}$ are acquired with the same integration time and excitation surface power. In this case, those parameters were set to 450 ms and 2.6 x 10^3 J/(s m^2), respectively. The excitation surface power was derived from the LED power (360 mW) and the excited area in the sample (⌀ = 25 mm) as a function of the transmission of the bandpass filter used to limit the LED emission (%T = 35).

The values obtained here are similar to the ones estimated from Figure S4, because the excitation surface energy are comparable in both measurements (PLQY and spectral resolved

PL) 25.2 x 10^3 J/m^2 and 5.7 x 10^3 J/m^2 respectively. All these values are summarized in Table S4:

Table S4. Summary of the contributions of fluorescence, phosphorescence and delayed fluorescence to the PLQY of biluminescent systems.

System	PLQY [%]	$PLQY_F$ [%]	$PLQY_D$ [%]	$PLQY_P$ [%]	A_{DF}	A_P
$[PMMA:NPB]_{sc}$	26±3	23.1	0.3	2.6	0.1	0.9
$[TCTA:NPB]_{sc}$	31±8	30.4	0.2	0.4	0.4	0.6
$[TCTA:NPB]_{evap}$	32±3	31.6	0.2	0.2	0.5	0.5

5. Experimental determination of the singlet and triplet population of the biluminescent system PMMA:NPB

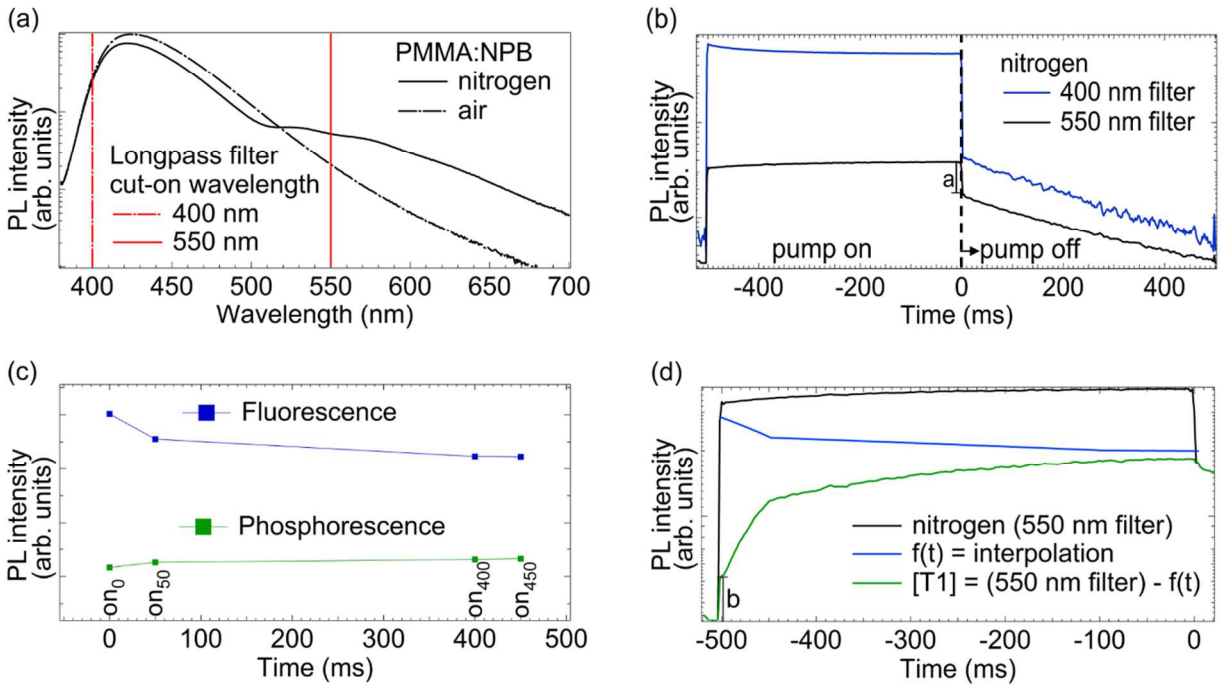

Figure S6. Experimental estimation of the singlet and triplet exciton densities of PMMA:NPB. (a) Photoluminescence spectra under continuous wave excitation, in both air (black dashed line) and nitrogen (black solid line). Red solid and dashed lines at 550 and 400 nm respectively, indicate the cut-on wavelengths of the longpass filters used during the time resolved experiments. (b) PL intensity during and after a 500 ms excitation pulse. The intensity was detected through a 400 nm (blue) and 550 nm (black) filters, suggesting the development of singlet and triplet populations during quasi-cw excitation pulses respectively. Constant "a" indicates the drop in fluorescence intensity immediately after the excitation source is off. (c) Intensities of fluorescence (380 – 500 nm) and phosphorescence (500 – 700 nm) obtained in 20 ms integration windows with different delays to the pump pulse start. Here, on_0 = no delay, on_{50} = 50 ms delay, on_{400} = 400 ms delay, and on_{450} = 450 ms delay. (d) Final profile of the triplet population evolution over time (green), as result of the subtraction of the interpolated fluorescence (blue) to the experimental data using the 550 nm filter (black). Here, [T1]=n_T. Constant "b" is attributed to the statistical error due to crosstalk between fluorescence and phosphorescence emissions.

We observed a correlation between the evolution of the measured PL intensity over time with the singlet and triplet densities of NPB. We chose the reference system PMMA:NPB to investigate this further.

In order to estimate experimentally the population of the singlet and triplet manifolds, we used time resolved photoluminescence measurements under nitrogen atmosphere. Long pass filters with cut-on wavelengths at 400 and 550 nm were used in front of the photodetector to selectively detect fluorescence and phosphorescence intensities respectively. However, the fluorescence emission extends to 700 nm (dashed black line in Figure S6a), so there is a fraction of fluorescence intensity which passes through the 550 nm filter, seen as the tail at the right side of the red solid line (cf. Figure S6a). This induces a contribution of the fluorescence in the measurement which aims to detect the phosphorescence emission. Such fluorescence contribution is observed in the PL transient measurement with the 550 nm filter (black solid line in Figure S6b) as the drop of intensity at "time=0" (when excitation pump is switched off), and it is labeled as "a" (cf. Figure S6b).

Figure S6c shows the PL response over time of the PMMA:NPB samples as they were exposed to 500 ms on, 500 ms off cycles quasi-cw pulse. When "pump on" the intensity over time of the fluorescence decreases (blue solid line) and at the same time the phosphorescence increases (black solid line), suggesting a profile of the singlet and triplet population density until a steady state is reached, before the excitation pulse is off. This result was reproduced as obtained from spectrally resolved time-gated measurements (cf. Figure S6c). Here, the intensities of fluorescence (380 – 500 nm) and phosphorescence (500 – 700 nm) were obtained in 20 ms integration windows with different delays to the starting point of the excitation pulse, where, on_0 = no delay, on_{50} = 50 ms delay, on_{400} = 400 ms delay, and on_{450} = 450 ms delay.

A profile which is closer to the population density of the triplet state n_T is shown in Figure S6d (green line). Here, the increase in intensity represents the increase of triplets over time while the molecules are pumped, it starts to decrease from "time=0" once the pump is off. Since there is a contribution of the fluorescence intensity in the phosphorescence measurements, n_T can be estimated if: The fluorescence data points in Figure S6c are interpolated to get a singlet density function "f(t)" (blue line, Figure S6d), which is normalized to the leaked fluorescence intensity "a" and subtracted to the measured phosphorescence (black line, Figure S6d), as expressed in:

$$n_{T\_experimental} \propto I_{phosphorescence} - I_{leaked\_fluorescence} \quad (6)$$

Where n_T experimental is the experimental population density of the triplet state, $I_{phosphorescence}$ is the measured intensity using the 550 nm longpass filter, and $I_{leaked\_fluorescence}$ is the fraction of fluorescence intensity above 550 nm which influences the measured intensity considered as the phosphorescence emission.

The triplet density related to the phosphorescence intensity does not start at zero. The remaining intensity "b" is attributed to the statistical error of the post-processing, needed due to the overlap between fluorescence and phosphorescence emission of the biluminescent emitter NPB.

Supporting references

(1) Kojima, I.; Li, B. Structural Characterization of Thin Films by X-Ray Reflectivity. *Rigaku. J*. **1999,** *16*, 31- 42.

(2) Xing, X.; Zhong, L.; Zhang, L.; Chen, Z.; Qu, B.; Chen, E.; Xiao, L.; Gong. Q. Essential Differences of Organic Films at the Molecular Level Via Vacuum Deposition

and Solution Processes for Organic Light Emitting Diodes. *J. Phys. Chem. C.* **2013,** *117*, 25405–25408.

(3) Griffiths, P. R.; De Haseth, J. A. Fourier Transform Infrared Spectrometry; Wiley: New Jersey, U.S.A., 2007.

(4) Reineke, S.; Walzer, K.; Leo, K. Triplet-Exciton Quenching in Organic Phosphorescent Light-Emitting Diodes with Ir-Based Emitters. *Phys. Rev. B*. **2007,** *75*, 125328.

(5) Reineke, S.; Schwartz, G.; Walzer, K.; Falke, M.; Leo, K. Highly Phosphorescent Organic Mixed Films: The Effect of Aggregation on Triplet-Triplet Annihilation. *Appl. Phys. Lett.* **2009,** *94*, 163305.